Numerical Modeling of Cell Differentiation and Proliferation in Force-Induced Substrates via Encapsulated Magnetic Nanoparticles

S.J. Mousavi and M.H. Doweidar*

Group of Structural Mechanics and Materials Modelling (GEMM), Aragón Institute of Engineering Research (I3A), University of Zaragoza, Zaragoza, Spain.
Mechanical Engineering Department, School of Engineering and Architecture (EINA), University of Zaragoza, Zaragoza, Spain.
Biomedical Research Networking Center in Bioengineering, Biomaterials and Nanomedicine (CIBER-BBN), Zaragoza, Spain.
* *Corresponding author e-mail address: mohamed@unizar.es*

Abstract

Cell migration, differentiation, proliferation and apoptosis are the main processes in tissue regeneration. Mesenchymal Stem Cells (MSCs) have the potential to differentiate into many cell phenotypes such as tissue- or organ-specific cells to perform special functions. Experimental observations illustrate that differentiation and proliferation of these cells can be regulated according to internal forces induced within their Extracellular matrix (ECM). The process of how exactly they interpret and transduce these signals is not well understood. Therefore, a previously developed three-dimensional (3D) computational model is here extended and employed to study how force-free substrates (FFS) and force-induced substrate (FIS) control cell differentiation and/or proliferation during the mechanosensing process. Consistent with experimental observations, it is assumed that cell internal deformation (a mechanical signal) in correlation with the cell maturation state directly triggers cell differentiation and/or proliferation. ECM is modeled as Neo-Hookean hyperelastic material assuming that cells are cultured within 3D nonlinear hydrogels. In agreement with wellknown experimental observations, the findings here indicate that within neurogenic (0.1-1 kPa), chondrogenic (20-25 kPa) and osteogenic (30-45 kPa) substrates, MSC differentiation and cell proliferation can be precipitated by inducing the substrate with an internal force. Therefore, cells require a longer time to grow and maturate within force-free substrates than withen force-induced substrates. In the instance of MSC differentiation into a compatible phenotype, the magnitude of the net traction force increases within chondrogenic and osteogenic substrates while it reduces within neurogenic substrates. This is consistent with experimental studies and numerical works recently published by the same authors. However, in all cases the magnitude of the net traction force considerably increases at the instant of cell proliferation because of cell-cell interaction. Consequently, the present model provides new perspectives to delineate the role of force-induced substrates in remotely controlling the cell fate during cell-matrix interaction, which open the door for new tissue regeneration methodologies.

Keywords: differentiation and proliferation; force-induced matrices; mechanosensing; numerical simulation; finite element method.

1. Introduction

The ability of Stem Cells (SCs) to differentiate into multiple cell types allows multiple tissues to be generated and reconstituted from a single cell source. Despite the advantages, the results may sometimes be disastrous if SCs differentiate at an inappropriate place and time or into undesirable phenotypes. This can lead to a pathological state or non-functional tissue construction. To avoid such abnormal conditions, cells have to be particularized in such a way as to differentiate or proliferate in response to appropriate biological stimuli.

Experiments have shown that, besides other factors [58, 59], the mechanical structure of cellular micro-environments plays an important role in cell differentiation and proliferation [22, 23, 31, 67]. For instance, Mesenchymal Stem Cells (MSCs) differentiate into specific phenotypes with high sensitivity to the tissue rigidity where they reside in. The mechanical interaction between a cell and its Extracellular Matrix (ECM) is considered symbiotic. Although cells are able to remodel their surrounding micro-environment, the mechanical structure and characteristics of their surroundings can also regulate intracellular signaling. This mutually dependent relationship between cells and their surrounding matrices is often referred to as dynamic reciprocity [13]. Consequently, besides other cell reactions [38, 39, 41], cells may respond to changes in their mechanical environment, such as changes in matrix rigidity, by undergoing differentiation and/or proliferation [13, 43]. For instance, experiments have demonstrated that for soft matrices that resembling brain tissue (0.1-1 kPa) SCs differentiate to neurogenic cells, for intermediate matrices that mimicking cartilage tissue (20-25 kPa) they differentiate into chondrogenic cells, and comparatively hard matrices that mimic the tissue of collagenous bone (30-45 kPa) they differentiate into osteogenic cells [13, 26, 40, 55]. Although MSCs have demonstrated quicker differentiation and an increase in the proliferation rate when cultured on osteogenic substrates [40, 42], mechanical forces induced into their micro-environment can actively accelerate these processes [34, 35]. This has been attributed to

protein anchorage densities and configurations which are proportional to substrate stiffness and rigidity [14]. However, the process of how exactly mechanical force regulates the MSC lineage specification is not well-known [40].

The findings of Kurpinski et al. [34] indicate that mechanical strain due to force inducement increases MSC proliferation and plays an important role in MSC differentiation. They show that the differential cellular responses to an anisotropic mechanical environment in a force-induced micro-environment have important implications in tissue engineering and remodeling due to alterations in the signaling pathway. In another study, the same group demonstrates that these mechanical stimulations play unique and important roles in the regulation of MSCs at both transcriptional and post-transcriptional levels. In addition, they suggest that an accurate combination of micro-environmental cues may promote MSC differentiation [35].

Among the wide range of biomaterials employed as cell substrate for *in vitro* investigations, hydrogels are a relevant option. These are composed of water-swollen networks of cross-linked polymer chains. While hydrogel stiffness depends on factors such as its concentration and cross-linking, due to its nonlinear behaviour, the stiffness can be altered as a result of internal contractile forces exerted by cells or by another internal compressing and/or stretching forces exerted within it [1, 2]. Several approaches have been proposed in the literature to enhance the local stiffness of the hydrogel, including plastic compression [6], cross-linking techniques [3] and magnetic field alignment of collagen-based hydrogels [1]. A helpful alternative approach to remotely induce an internal force within hydrogels and to change their relative local stiffness is to incorporate magnetic nanoparticles within them. Inducing magnetic force on these magnetic nanoparticles causes compression and/or stretching of the hydrogel, leading to an increase in the bulk elastic modulus and the hydrogel rigidity.

Several numerical models have been developed for considering the general patterns of tissue reconstruction resulting from the external mechanical stimuli during fracture healing [9, 10, 21, 30, 32, 36, 37, 64]. For example, Stops et al. [64] have considered cell differentiation and proliferation within a collagen-glycosaminoglycan scaffold subjected to mechanical strain and perfusive fluid flow. Kang et al. [30] developed a model for bone fracture healing based on the density of different cell phenotypes by coupling cell differentiation and proliferation to the magnitude and frequency of the mechanical stimuli. Although these models are useful to predict tissue repairing, they consider neither cell differentiation and/or proliferation due to the mechanosensing process during cell substrate interaction nor the nonlinearity of cell micro-environment. A numerical model considering cell differentiation and proliferation based on the mechanosensing process within a force-free linear elastic substrate has been previously developed and presented by the present authors [47]. The main aim of the present work is to extend the previously presented model to include the effect of the nonlinearity of the hydrogel on cell differentiation and proliferation when an internal force is applied within the substrate.

2. Material and methods

2.1. ECM material behavior

Hydrogels are frequently used to study cell adhesion and responses to substrate stiffness. Since hydrogels become stiffer as they are strained, cell response strongly depends on the compression and tension loads applied in such substrates. This stiffening can be regulated by applying an internal force in the cell micro-environment to modulate and control its differentiation and proliferation [29, 52, 68]. A Neo-Hookean hyperelastic material model is here employed to model nonlinear behavior of hydrogel substrate materials undergoing deformations [17]. Although in this model the stress-strain relationship is initially linear, at a certain threshold the stress-strain curve reaches a plateau. The strain energy density function for a compressible neo-Hookean material in 3D can be expressed as [53]

$$W = C_1(I_1 - 3) + D_1(J-1)^2 \tag{1}$$

where C_1 and D_1 are material constants. To be consistent with linear elasticity $C_1 = G/2$ and $D_1 = \kappa/2$, G and κ are the shear modulus and the bulk modulus, respectively. I_1 is an invariant expressed in terms of the right Cauchy-Green tensor, $\mathbf{C} = \mathbf{F}^{\mathrm{T}}\mathbf{F}$, as $I_1 = tr(\mathbf{C})$ and $J = \det(\mathbf{F})$ is the Jacobian determinant, where $\mathbf{F} = \nabla x$ is the deformation gradient tensor.

Green strain and Cauchy stress are defined, respectively, as

$$\boldsymbol{\epsilon} = \frac{1}{2}(\mathbf{C} - \mathbf{I}) \tag{2}$$

$$\boldsymbol{\sigma} = 2J^{-1}\mathbf{F}\frac{\partial W}{\partial \mathbf{C}}\mathbf{F}^{\mathrm{T}} \tag{3}$$

Subsequently, the stiffness tensor can be written as

$$\mathbb{C} = 2\frac{\partial^2 W}{\partial \mathbf{C^2}} \tag{4}$$

2.2. Cells effective forces

Two main cellular elements regulate cell migration; active cellular elements, generated as a result of the overlap between actin filaments and myosin II, and passive cellular elements, arising due to the resistance of microtubules and the cell membrane. The former generates active contractile stress that mainly depends on the minimum, ϵ_{min} and the maximum, ϵ_{max}, cell internal strains, while the latter produces passive mechanical strength that is proportional to the passive cellular stiffness and the cell internal deformation. Therefore, by approximating each cellular element with a linear elastic spring, the net cell stress transmitted to the ECM can be calculated as [44, 45, 51]

$$\sigma_{\mathrm{cell}} = \begin{cases} & \epsilon_{\mathrm{cell}} < \epsilon_{\mathrm{min}} \\ \varphi & \text{or} \\ & \epsilon_{\mathrm{cell}} > \epsilon_{\mathrm{max}} \\ \varphi + \frac{\epsilon_{\mathrm{min}} - \epsilon_{\mathrm{cell}}}{\epsilon_{\mathrm{min}}\sigma_{\mathrm{max}}^{-1} - K_{\mathrm{act}}^{-1}} & \epsilon_{\mathrm{min}} \le \epsilon_{\mathrm{cell}} \le \epsilon^* \\ \varphi + \frac{\epsilon_{\mathrm{max}} - \epsilon_{\mathrm{cell}}}{\epsilon_{\mathrm{max}}\sigma_{\mathrm{max}}^{-1} - K_{\mathrm{act}}^{-1}} & \epsilon^* \le \epsilon_{\mathrm{cell}} \le \epsilon_{\mathrm{max}} \end{cases} \tag{5}$$

where $\varphi = K_{\mathrm{pas}}\epsilon_{\mathrm{cell}}$ and $\epsilon^* = \sigma_{\mathrm{max}}K_{\mathrm{act}}^{-1}$. K_{act}, σ_{max} and ϵ_{cell} represent the stiffness of passive and active cellular elements, the

maximum contractile stress exerted by the actin-myosin machinery and the internal strain of the cell, respectively.
Contraction of the actin-myosin apparatus drives forward the cell body due to the traction force generated by the cell. This force is proportional to the net stress transmitted by the cell to the substrate. Although the present model is applicable for any cell configuration [46, 51], we assume a spherical configuration for the sake of simplicity. So, using discrete finite element methodology and representing the cell by a connected group of finite elements, the nodal traction force can be expressed as [44, 48]

$$\mathbf{F}_i^{\text{trac}} = \sigma_{\text{cell}} S \zeta \mathbf{e}_i \tag{6}$$

where $\mathbf{e}_i$ represents a unit vector from the ith node of the cell membrane towards the cell centroid and S denotes the cell membrane area per node. ζ is "adhesivity" which can be defined as [48, 71]

$$\zeta = k n_r \psi \tag{7}$$

where k, n_r and ψ are the binding constant of the cell integrins, the total number of available receptors and the concentration of the ligands at the leading edge of the cell.
Therefore, the vector summation of all nodal traction forces delivers the net traction force $\mathbf{F}_{\text{net}}^{\text{trac}}$ acting on the whole cell membrane nodes [48, 46].
On the other hand, the drag force resists cell motility [46, 71]. The main objective here is to define a velocity-dependent opposing force associated with the viscous character of the substrate. Referring to Stokes' drag regime, the drag force acting on a spherical cell can be presented as [48, 71]

$$F_{drag} = 6\pi r \eta v \tag{8}$$

where r and v are cell radius and velocity, respectively, while η is medium viscosity. Cells send out local protrusions to probe their environment by exerting a random protrusion force. This is generated by actin polymerization, distinguished from the cytoskeletal contractile [71]. This causes cells to move along a directed random path following the effective signal. Therefore, the direction and magnitude of the protrusion force are chosen randomly at each time step. It is worth noting that the order of the protrusion force magnitude is the same as that of the traction force but with a lower amplitude [28, 48, 71]. So, it can be described as

$$\mathbf{F}_{\text{prot}} = \alpha F_{\text{net}}^{\text{trac}} \mathbf{e}_{\text{rand}} \tag{9}$$

where $\mathbf{e}_{\text{rand}}$ and α represent a random unit vector and a random scalar, $0 \leq \alpha < 1$, respectively, while $F_{\text{net}}^{\text{trac}}$ is the magnitude of the net traction force [48, 49]. At the microscale, the viscous resistance dominates the inertial resistance [48, 71] so that the force balance reads

$$\mathbf{F}_{\text{net}}^{\text{trac}} + \mathbf{F}_{\text{prot}} = \mathbf{F}_{\text{drag}} \tag{10}$$

2.3. Mechanosensing and cell reorientation

Guided by experimental observations [41, 15], it is considered that first the cell exerts sensing forces on the cell-substrate interface to diagnose its surrounding micro-environment. It is assumed that these forces act at each finite element node of the membrane towards the cell centroid. Therefore, the cell internal strain at each finite element node of the cell membrane can be written as

$$\epsilon_{\text{cell}} = \mathbf{e}_{\text{i}} : \boldsymbol{\epsilon}_i : \mathbf{e}_{\text{i}}^{\text{T}} \tag{11}$$

where $\boldsymbol{\epsilon}_i$ represents the strain tensor of the ith node located on the cell membrane in the mechanosensing process. Subsequently, the cell polarisation direction $\mathbf{e}_{\text{pol}}$ can be calculated from Eq. 10 as the unit victor in the direction of $\mathbf{F}_{\text{drag}}$. From Eq. 8 and Eq. 10, the cell velocity can be defined as

$$v = \frac{\| \mathbf{F}_{\text{drag}} \|}{6\pi r \eta} \tag{12}$$

Subsequently, during time step, τ, the translocation vector of the cell through which the cell migrates to a new position can be defined as

$$\mathbf{d} = v\tau \mathbf{e}_{\text{pol}} \tag{13}$$

2.4. Cell-cell interaction

In reality cells inside a multicellular system do not preserve a spherical shape but deform so as to be tangent to each other during migration [56]. So, to avoid interference between two cells, a useful simplification here is to consider $\|\mathbf{x}_{ij}\| \geq 2r$, where $\mathbf{x}_{ij}$ is a vector passing through the centroid of two cells i and j (see Fig. 1).
In vivo, the cell sends out pseudopods to sense its microenvironment. When two or more cells come into contact with each other, common vertices of the cells (for instance vertices n_1:n_4 in Fig. 1) engage each other so that the cell cannot send out any pseudopod in those vertices [5, 65]. Therefore, in this condition, it is assumed that cells are not able to exert any sensing force at those common vertices. Although in such a situation the vertices in contact never play any role in the mechanosensing process, the nodal traction forces are not zero in those vertices [48, 50].

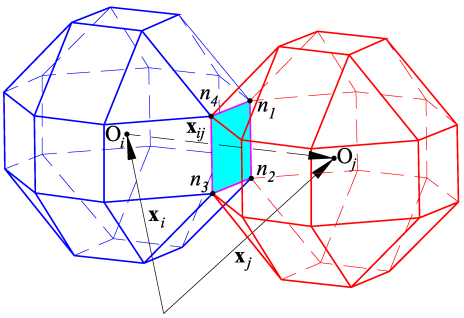

Figure 1: Interaction of two cells in contact. For the assumed cell configuration, two cells can have a maximum of four common vertices (n_1:n_4). $\mathbf{x}_{ij}$ represents a vector passing by the centroids of the ith (O_i) and jth (O_j) cells with position vectors of $\mathbf{x}_i$ and $\mathbf{x}_j$, respectively. To avoid the interference of two cells it is considered that $\|\mathbf{x}_{ij}\| \geq 2r$.

2.5. Cell differentiation, proliferation and apoptosis

Cells may respond to the mechanical properties of their ECM, such as substrate stiffness, by differentiation, proliferation and/or apoptosis [22, 23, 31, 67]. Experiments demonstrate that a specific deformation range sensed by a cell leads to

a specific differentiation [10, 34, 69]. This refers to distinguishing between their original tissue, the magnitude and duration of the mechanical signal received by the cell and the degree of preconditioning. Besides, experiments show that cell apoptosis may occur because of the deformation threshold which is durable for a typical cell [22, 31]. Experimental observations by Kearney et al. [31] indicate that tensile strain induced on MSCs mediates cell apoptosis. For instance, the findings of Gladman et al. [22] indicate that, depending on the duration of the imposed strain, injury beyond 20% of the tensile cyclic strain leads to significant neuronal cell death.

Here, it is considered that MSCs are prone to differentiate into a certain cell type i, where $i \in \{s, c, l\}$ represents lineage specifications of osteoblasts, s, chondrocytes, c, and neuroblasts, l. Mechano-regulation of differentiation is introduced in terms of cell internal deformation in the cell polarisation direction. Deformation of each node located on the cell membrane in the cell polarisation direction can be calculated as [47]

$$\gamma_i = \mathbf{e}_{\text{pol}} : \boldsymbol{\epsilon}_i : \mathbf{e}_{\text{pol}}^{\text{T}} \tag{14}$$

Subsequently, cell internal deformation, which varies temporally and spatially [10, 30, 60], in the cell polarisation direction can be obtained by

$$\gamma(\mathbf{x}, t) = \sum_{i=1}^{n} \gamma_i \tag{15}$$

where n is the number of nodes located on the cell membrane.

On the other hand, experimental observations illustrate that cell differentiation and proliferation are time-dependent [12, 11, 70]. For instance, it is well known that MSCs [12] and chondrocyte [70] need a certain time to become sufficiently mature to undergo differentiation or proliferation. Therefore, according to this argument, the cell differentiation and proliferation is linked also to a maturation time, the time that the cell needs to be active in the differentiation and/or proliferation stage [30, 11]. This maturation period is different for every cell type and can be moderated via the mechanical signals received by a typical cell. Stronger mechanical signals (less internal deformation) decrease the cell maturation time, increasing the differentiation or proliferation rate. However, after cell culture, even within hydrogels that produce the strongest mechanical signals, cells need a minimum time period to start differentiation or proliferation [11]. Therefore, it is assumed that the cell maturation time is linearly proportional to the internal deformation as

$$t_{\text{mat}}(\gamma, t) = t_{\text{min}} + t_{\text{p}}\gamma(\mathbf{x}, t) \tag{16}$$

where t_{min} is the minimum time required by a typical cell to differentiate or proliferate while t_{p} is a time proportionality. Therefore, beside lineage specifications $i \in \{m, s, c, l\}$ (m represents the MSC phenotype), each cell type is also represented by a Maturation Index (MI) described as [47]

$$\text{MI} = \begin{cases} \frac{t}{t_{\text{mat}}} & t \le t_{\text{mat}} \\ 1 & t > t_{\text{mat}} \end{cases} \tag{17}$$

MI=1 means that a typical cell is fully mature and is ready to differentiate or proliferate if it receives the appropriate mechanical signal. MI=0 indicates a young cell, which means that the cell is not yet able to start the differentiation or proliferation process, even in the presence of the appropriate mechanical stimulus. It is assumed that the evolution of cell MI is an irreversible process. Considering these conditions, the process of MSC differentiation and apoptosis can be related to mechanical signals and maturation as [30, 47]

$$\text{Cell phenotype} = \begin{cases} s & \gamma_{\text{l}} < \gamma \le \gamma_s \ \&\ \text{MI} = 1 \\ c & \gamma_s < \gamma \le \gamma_c \ \&\ \text{MI} = 1 \\ l & \gamma_c < \gamma \le \gamma_{\text{u}} \ \&\ \text{MI} = 1 \\ \text{apoptosis} & \gamma_{\text{apop}} < \gamma \\ \text{no diffrentiation} & \text{otherwise} \end{cases} \tag{18}$$

where γ_{l} and γ_{u} are lower and upper bounds of cell internal deformations, respectively. It is worth noting that small strains exerted cyclically on a typical cell may cause fatigue apoptosis of the cell [31] which is not included in the present model.

Cell proliferation is the process of generating two daughter cells from a single mother. It occurs in four defined steps comprising the first growth phase, the synthesis phase, the second growth phase and the mitosis phase, respectively [18, 66]. During the first growth phase (G1) the cell synthesizes biological material in order to grow. Then the cell enters the synthesis phase (S) to replicate the sister chromatids. Afterwards, the second growth phase (G2) provides time for proofreading to ensure the DNA is properly replicated and packaged prior to cell division. Finally, cell division (cytokinesis) occurs and a mother cell is divided into two daughter cells in the mitosis phase (M). In this critical phase some cells may temporarily stop proliferation and enter into the quiescence state (G0) while others participate in the cycle of cell proliferation [18, 66].

The main objective here is to model the proliferation process through a biologically proper environment. Therefore, it is assumed that there are no concerns about nutrients or oxygen shortage for the cells in culture. The dominant phases of cell division are modeled by splitting the cell proliferation cycle into two main steps. It is hypothesized that during the G1, S and G2 phases the cell grows and matures in such a way that if a fully mature cell receives an appropriate mechanical signal, one mature mother cell enters into the M phase and is divided into two non-mature daughter cells. Therefore, in the present model, the cell is either under maturation or in the proliferation phase as [47]

$$\text{Cell growth} = \begin{cases} \text{cell division} & \gamma \le \gamma_i^{\text{prof}} \ \&\ \text{MI} = 1 \\ \text{no cell division} & \text{otherwise} \end{cases} \tag{19}$$

where $i \in \{m, s, c, l\}$ and $\gamma_i^{\text{prof}} < \gamma_{\text{u}}$ is the maximum internal deformation that can lead to proliferation of cell i [30]. When a mother cell is divided into two daughter cells, it is assumed that one of the daughter cells is located in the same position as the mother cell, $\mathbf{x}_{\text{daut}}^{(1)} = \mathbf{x}_{\text{moth}}$, while the other is located in the vicinity of the mother cell, $\mathbf{x}_{\text{daut}}^{(2)} = \mathbf{x}_{\text{moth}} + 2r\mathbf{e}_{\text{rand}}$. The "moth" and "daut" subscripts represent mother and daughter cells, respectively, while $\mathbf{e}_{\text{rand}}$ denotes a random unit vector.

Table 1: General parameters employed in the model except where other values are specified.

Symbol	Description	Value	Ref.
η	Minimum substrate viscosity	1000 Pa.s	[4, 71]
K_{pas}	Stiffness of microtubules	2.8 kPa	[62]
K_{act}	Stiffness of myosin II	2 kPa	[62]
ϵ_{max}	Maximum strain of the cell	0.9	[48, 61]
ϵ_{min}	Minimum strain of the cell	-0.9	[48, 61]
σ_{max}	Maximum contractile stress exerted by actin-myosin machinery	0.1 kPa	[54, 57]
$k_f = k_b$	Binding constant at rear and front of the cell	10^8 mol^{-1}	[71]
n_{r_f}	Number of available receptors at the front of the cell	1.5×10^5	[71]
n_{r_b}	Number of available receptors at the back of the cell	10^5	[71]
ψ	Concentration of the ligands at rear and front of the cell	10^{-5} mol	[71]
t_{min}	Minimum time needed for cell proliferation	4 days	[11, 30]
t_{p}	Time proportionality	200 days	[11, 30]
γ_{l}	Lower bound of cell internal deformation leading to osteoblast differentiation	0.005	[27, 30]
γ_{s}	Upper bound of cell internal deformation leading to osteoblast differentiation	0.04	[27, 30]
γ_{c}	Upper bound of cell internal deformation leading to chondrocyte differentiation	0.1	[30]
γ_{u}	Upper bound of cell internal deformation leading to neuroblast differentiation	0.5	
γ_{apop}	Cell internal deformation leading to cell apoptosis	1	[30]
γ_i^{prof}	Limit of cell proliferation	0.2	[30]

3. Finite element implementation

The present nonlinear constitutive model is implemented in the commercial Finite Element (FE) software ABAQUS [25] through a coupled user-defined element (UEL). The developed model is applied in several numerical examples to study cell differentiation and proliferation within force-free and force-induced substrates with different degrees of stiffness. It is assumed that the cell is located within a substrate with dimensions of 1000×500×500 μm, far from the boundaries of the matrix in such a way that there is no effect of the boundary conditions on the cell behavior. To remotely exert an internal force within the substrate, it is assumed that magnetic nanoparticles are encapsulated in a hard sphere with the same cell's radius and embedded in the center of the substrate. The matrix is meshed by 128,000 regular hexahedral elements and 136,161 nodes. The calculation time is about one minute for each time step, corresponding to approximately 6 hr of real cell-matrix interaction [47]. Initially the cell is assumed to have a spherical shape. The properties of the matrix and the cell are enumerated in table 1.

4. Results

4.1. Force-induced substrate deformation

In vivo, cells are continuously subjected to mechanical forces that, among other cues, are believed to control their growth and lineage specification. These mechanical forces, directly applied to the substrate, cause strain transfer into the cells through either focal adhesions or membrane. *In vitro*, there are several methods by which a force can be imposed within the cell substrate, such as encapsulated magnetic nanoparticles or using bioreactor systems [3, 33, 63]. Here, it is assumed that there are magnetic nanoparticles encapsulated within a rigid sphere located in the middle of the substrate. Initially, the substrate stiffness is set to lower bounds of neurogenic (0.1-1 kPa), chondrogenic (20-25 kPa) and osteogenic cells (30-45 kPa) tissue stiffness [8]. Then, cell-cultured hydrogel is induced by a force in the longitudinal direction to increase the substrate rigidity. For example, Fig. 2 shows osteogenic substrate deformation due to an applied traction force of 5 μN. As seen in Fig. 2-a, the left and right hand sides of the rigid sphere undergo tensile and compressive deformations, respectively. Thus, pores in those regions are elongated in longitudinal and lateral directions, respectively, (Fig. 2-b). Although in this situation the direction of the pores is different in the two regions, the pore density in both regions is the same [63]. Consequently, the cell behavior in both regions under compression or tension is identical since the cell feels the same rigidity as seen in Fig. 2-c.

4.2. MSC proliferation and differentiation within force-free osteogenic substrate

The present model is applied to study MSC proliferation and differentiation in a substrate with nonlinear behaviour such as hydrogel. Fig. 3 represents the MSC response when it interacts with a nonlinear substrate within the range of osteogenic like tissue stiffness. Initially, it is assumed that a MSC is located near to a rigid sphere while no internal force is applied to the substrate. As the MSC maturates in a force-free osteogenic substrate, one mature mother MSC proliferates delivering two daughter cells in a non-mature state after ~9.75 days (Fig. 3-a). Subsequently, maturation of new mesenchymal daughter cells may be followed by differentiation or proliferation, depending

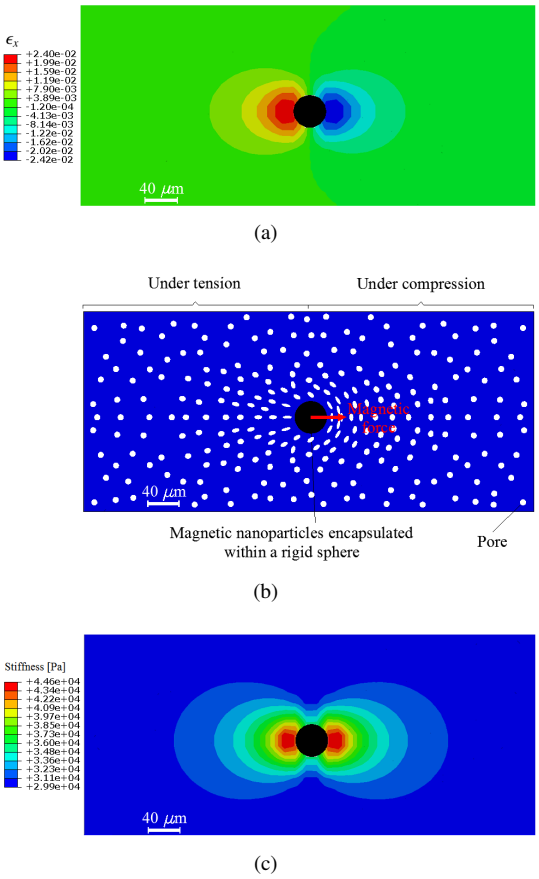

Figure 2: Osteogenic substrate deformation induced by an internal force (5 μN) using magnetic nanoparticles encapsulated within a rigid sphere. a- The right hand side of the rigid sphere is under compression and the left side is under tension. b- Schematic diagram of pores deformation around encapsulated nanoparticles. Pores in two different regions of the substrate under tension and compression is elongated in longitudinal and lateral directions, respectively, while the porosity is the same in both sides. c- Distribution of substrate stiffness [Pa] after force inducement.

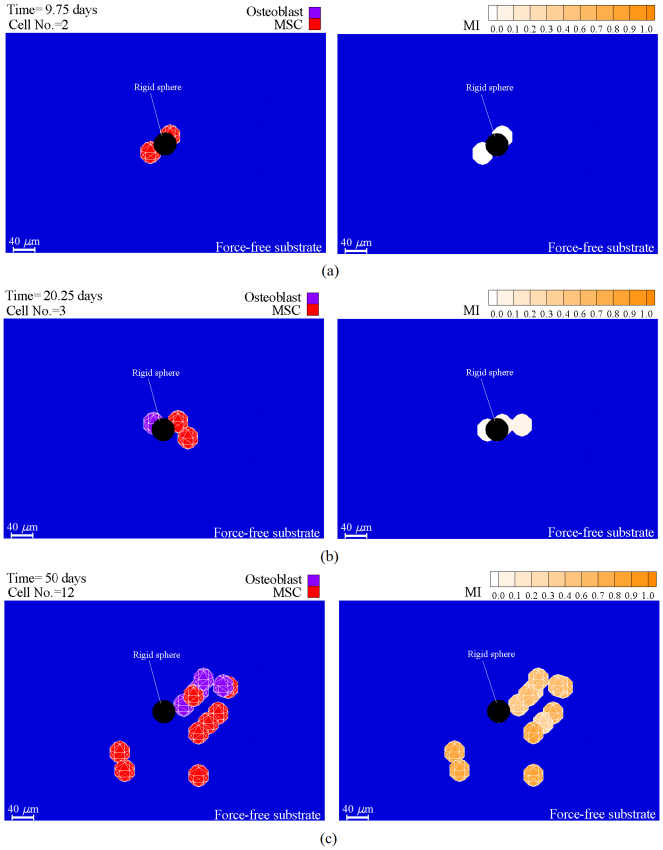

Figure 3: MSC proliferation and differentiation within a force-free osteogenic substrate. a- The initial moment of MSC proliferation, b- the initial moment of MSC differentiation into osteoblast and c- the continuation of MSC differentiation and proliferation of MSCs and osteoblasts.

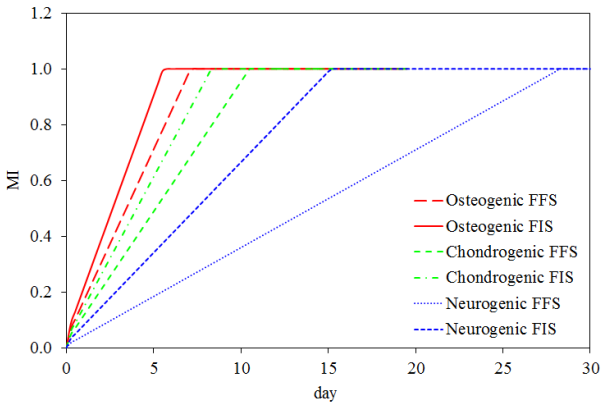

Figure 4: MI of MSCs within substrates with different characteristics. FFS and FIS stand for force-free and force-induced substrates, respectively.

on the mechanical signal, γ, received by the cells. Afterwards, initial MSC differentiation occurs after ~20.25 days (Fig. 3-b) and the process is followed by MSC differentiation and proliferation of both MSC and osteoblast (Fig. 3-c). Likewise, as in the linear elastic model previously presented by the same authors [47], there is a sudden considerable jump in the average net traction force in the instance of MSC differentiation and proliferation (Fig. 5). This is qualitatively consistent with the observations of Fu et al. [20]. In the case of MSC differentiation, this is attributed to the quality of the ECM and the adhesion of a typical cell [72]. In the case of cell proliferation, this occurs due to cell-cell interaction which causes an asymmetric distribution of the internal cell deformation [47, 50].

4.3. MSC lineage specification within force-free and force-induced osteogenic substrates

Here two different numerical examples are designed to study the lineage specification of MSCs in osteogenic substrates. To avoid repeating MSC proliferation, the results are represented starting from the instant of MSC differentiation. First, it is considered that the substrate stiffness is equal to the lower bound of osteogenic substrates (30 kPa) [8] without inducing any internal force within the substrate. In order to study the effect of force-induced substrate, an internal force (5 μN) is applied in the middle of the substrate in the longitudinal direction which increases the substrate local stiffness around a rigid sphere. The differentiation of MSCs into osteogenic phenotype for both cases is presented in Fig. 6. During cell-substrate interaction, MSC is grad-

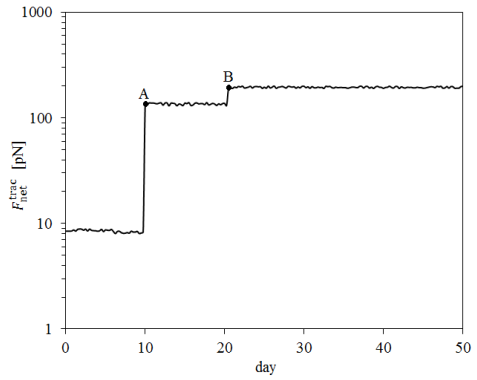

Figure 5: Average cell traction force within a force-free osteogenic substrate. Average cell traction force, F_{net}^{trac}, versus time within a force-free osteogenic substrate during MSC proliferation and differentiation. Point A represents the instant of MSC proliferation which causes a considerable jump in the average net traction force while point B is the initial instant of MSC differentiation into osteoblast resulting in an increase in the average net traction force.

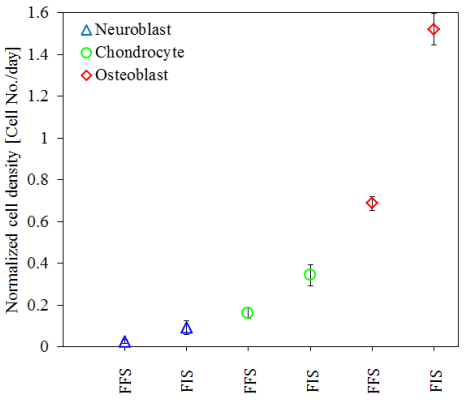

Figure 7: Normalized density of a typical cell in substrates with different characteristics during identical times as a consequence of MSC differentiation and proliferation of each cell phenotype. The error bars represent mean standard deviation of different runs. FFS and FIS stand for force-free and force-induced substrates, respectively.

ually maturated. Once it is completely mature (MI=1), it differentiates into osteoblast within force-free and force-induced substrates after ~7.25 days and ~5.75 days, respectively. MSC differentiation within a substrate with a stiffness resembling that of osteogenic tissue is observed in many experimental findings [13, 16, 26]. MSC differentiation into osteoblast is followed by osteoblast proliferation after ~ 14.75 and ~ 11.75 days in force-free and force-induced substrates, respectively. So, each new osteoblast may again proliferate into many osteoblasts when both the strength of the mechanical signal received by the cell and its maturation state are appropriate (see Figs. 6-a and 6-b). Comparing the density of each cell phenotype in Fig. 7 and taking into account the results in Figs. 6, it can be seen that MSC differentiation and proliferation of osteoblasts is accelerated within force-induced substrate. This is due to the decrease in the cell maturation time when the substrate is induced with an internal force (see also Fig. 4). The expedition of MSC differentiation into osteoblast within force-induced substrates is consistent with wellknown experiments [34, 35]. It is worth noting that, as shown in the previous work of the same authors [47], in both cases MSC differentiation into osteoblast as well as osteoblast proliferation lead to an instant increase in the average magnitude of the net traction force (results are not shown here), consistent with the experimental findings of Fu et al. [20].

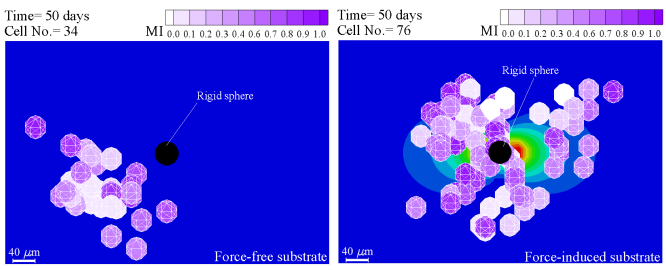

Figure 6: Osteoblast proliferation in osteogenic substrates. a- Force-free osteogenic substrate (see also V1 Video) and b- force-induced osteogenic substrate (see also V2 Video).

4.4. MSC lineage specification within force-free and force-induced chondrogenic substrates

To study the fate decision of MSCs within force-free and force-induced chondrogenic substrates, two simulations are performed here. Again, to avoid the demonstration of the MSC proliferation process, the results are presented starting from the moment of MSC differentiation. The substrate stiffness is set to be the lower bound of chondrogenic tissue stiffness (20 kPa) [8] and it is induced by a 3 μN force in the longitudinal direction. MSC located near the rigid sphere is gradually maturated. Within force-free and force-induced chondrogenic substrates, completely mature MSC starts to differentiate into chondrocyte after ~ 10.25 and ~ 7.75 days, respectively. As seen in Fig. 8, as the new cell phenotype is mature when the mechanical signal is appropriate, it proliferates into many chondrocytes. However, according to Figs. 7 and 8 the density of chondrocytes within the force-induced chondrogenic substrate (cell no.=8) is greater than the force-free one (cell no.=17). Our findings, consistent with experimental observations, indicate that differentiation and proliferation processes are accelerated within a force-induced chondrogenic substrate due to the increase in the matrix stiffness within the range of chondrogenic tissue stiffness [34, 35]. This is due to the increase in the substrate rigidity and consequently a decrease in the cell maturation time [7] (Fig. 4). Furthermore, consistent with the observations of of Fu et al. [20], MSC differentiation into chondrocyte produce a jump in magnitude of the net traction force. As a consequence of chondrocyte proliferation and its associated cell-cell interaction, the average magnitude of the net traction force increases (results are not shown here).

4.5. MSC lineage specification within force-free and force-induced neurogenic substrates

Experimental observations demonstrate that MSC culture within substrates resembling neurogenic tissue leads to neural precursor cells [13, 24]. As in the previous examples, the

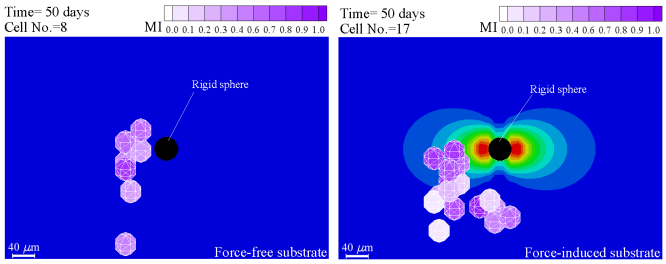

(a) (b)

Figure 8: Chondrocyte proliferation within chondrogenic substrates. a- Force-free chondrogenic substrate (see also V3 Video) and b- force-induced chondrogenic substrate (see also V4 Video).

results starting from the instant of cell differentiation are presented. MSC is located around a rigid sphere within a substrate with stiffness of the lower bound of neurogenic tissue (0.1 kPa) [8] and then a 0.1 μN force is applied in the longitudinal direction to increase the substrate local stiffness. The results of MSC differentiation and proliferation of neuroblasts are shown in Fig. 9. When MSC is maturated, it differentiates into neuroblast within both force-free and force-induced substrates. However, as in previous numerical examples, differentiation is quicker in the case of force-induced neurogenic substrates (after $\sim$ 28.5 days and $\sim$ 25.5 days for force-free and force-induced substrates, respectively). The acceleration of MSC differentiation due to the increase in the substrate stiffness within relatively soft substrates is observed by Fu et al. [20] in the case of adipoblasts. MSC differentiation into neuroblast causes a decrease in the magnitude of the net traction force, which was observed in the previous experimental [20] and numerical [47] works. This is because, within a neurogenic substrate, MSCs are more contractile than neuroblasts. Afterwards, MSC differentiation is followed by proliferation of neuroblasts into several cells within force-free and force-induced substrates. As concluded from Figs. 7 and 9, within a force-induced substrate neuroblast density is higher, which means that its proliferation is quicker. This occurs because the stimulation of the substrate by an internal force increases the substrate rigidity and in turn advances the instant of cell maturation (see Fig. 4). In this case, as in the previous ones, the cell-cell interaction increases the average magnitude of the net traction force due to neuroblast proliferation (data are not presented here).

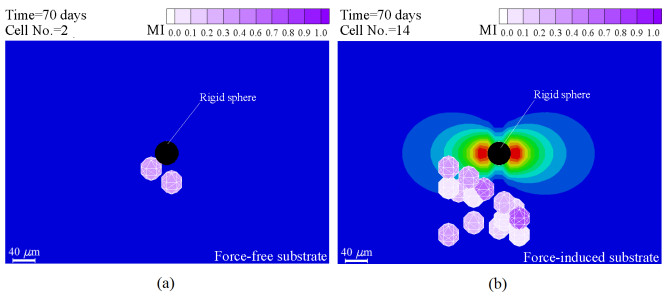

(a) (b)

Figure 9: Neuroblast proliferation within neurogenic substrates. a- Force-free neurogenic substrate (see also V5 Video) and b- force-induced neurogenic substrate (see also V6 Video).

5. Conclusions

MSCs are self-renewing and have significant potential to undergo lineage specification. Many studies [13, 34, 35, 40] have been devoted to achieving a better understanding of the mechanisms which regulate the lineage specification of these cells. Recent experimental studies demonstrate that the mechanical properties of cell micro-environments and the stimulation of the micro-environment by an external force trigger many aspects of cell response such as differentiation and proliferation [13, 40]. Although the precise mechanical pathway by which the cell micro-environment controls the cell differentiation and proliferation is not still well-known, various hypotheses have been proposed to clarify how mechanical signals regulate cell fate [10, 40].

Recently, a 3D numerical model was developed by the same authors to study the influence of substrate stiffness on cell fate [47]. To acquire accurate control over cell differentiation and proliferation, the previous model is extended to investigate the effects of substrate induced internal force on cell fate. We believe that this is the first nonlinear numerical model to interpret existent knowledge of cell fate when the cellular micro-environment is induced by a substrate internal force.

In this study, we have investigated how 3D force-free and force-induced substrates affect cell proliferation and differentiation of MSCs. The results are qualitatively consistent with experimental observations [13, 16, 20, 26, 34, 35, 72]. We found that for a typical cell, cell internal deformation, which is developed through integrins during focal adhesions, is a key molecular mechanism in the mechanosensing process. Therefore, any change in the substrate rigidity due to a matrix induced internal force changes the cell internal deformation which in turn moderates the cell proliferation and differentiation [19, 34]. This is why within a substrate stimulated by an internal force, cell differentiation and proliferation is accelerated [16, 35]. In line with our previous work [47] and experimental observation [20], in the case of force-free and force-induced substrates, the net traction force generated by a typical cell may lead to a sudden increase (osteoblasts and chondrocytes) or decrease (neuroblast) in the moment of MSC differentiation. This sudden jump or drop in the net traction force may be due to the perfect alignment of stress fibers of the cell when the matrix and the cell stiffness are similar at the moment of MSC differentiation. Moreover, in all cases considered here, proliferation of a typical cell significantly increases the average net traction force. This is due to the cell-cell interaction which results in an asymmetric distribution of the traction force on the cell membrane, as discussed in [45]. In addition, the cell behavior in terms of cell differentiation or proliferation strongly depends on the cell maturation. Consistent with the observations of Hera et al. [24], our findings illustrate that cells might need a longer time to become fully mature within force-free substrates (see Fig. 4) which is another reason for quicker cell fate achievement within force-induced substrates.

Altogether, the results obtained from the present model, in agreement with the previous experimental observations [16, 20, 34, 35, 72], show that internal force exerted within the cell

micro-environment can play an outstanding role in remotely controlling the lineage specification of MSCs and cell proliferation, which open the door for new tissue regeneration methodologies. Although this 3D numerical model can successfully predict fundamental aspects of cell maturation, differentiation, proliferation and apoptosis within nonlinear substrate, further investigations into physical and mechanical factors such as colony size and cell shape are essential for a better understanding of the precise mechanism behind cell fate decisions.

6. Acknowledgements

The authors gratefully acknowledge the financial support from the Spanish Ministry of Economy and Competitiveness (MINECO MAT2013-46467-C4-3-R), the Government of Aragon (DGA) and the CIBER-BBN initiative. CIBER-BBN is financed by the Instituto de Salud Carlos III with assistance from the European Regional Development Fund.

References

[1] M. Ahearne. Introduction to cell-hydrogel mechanosensing. *Interface Focus*, 4:20130038, 2014.

[2] M. Ahearne, S.L. Wilson, K.K. Liu, S. Rauz, A.J. El Haj, and Y. Yang. Influence of cell and collagen concentration on the cell-matrix mechanical relationship in a corneal stroma wound healing model. *Exp. Eye Res.*, 91:584–591, 2010.

[3] M. Ahearne, Y. Yang, K.Y. Then, and K.K. Liu. Nondestructive mechanical characterisation of UVA/riboflavin crosslinked collagen hydrogels. *Br. J. Ophthalmol*, 92:268–271, 2008.

[4] S.K. Akiyama and K.M. Yamada. The interaction of plasma fibronectin with fibroblastic cells in suspension. *Journal of Biological Chemistry*, 260(7):4492–4500, 1985.

[5] G.W. Brofland and C.J. Wiebe. Mechanical effects of cell anisotropy on epithelia. *Computer Methods Biomech. Biomed. Engin.*, 7(2):91–99, 2004.

[6] R.A. Brown, M. Wiseman, C.B. Chuo, U. Cheema, and S.N. Nazhat. Ultrarapid engineering of biomimetic materials and tissues: fabrication of nano- and microstructures by plastic compression. *Adv Funct Mater*, 15:1762–70, 2005.

[7] D.P. Burke and D.J. Kelly. Substrate stiffness and oxygen as regulators of stem cell differentiation during skeletal tissue regeneration: A mechanobiological model. *PLoS ONE*, 7(7):e40737, 2012.

[8] A. Buxboim, I.L. Ivanovska, and D.E. Discher. Matrix elasticity, cytoskeletal forces and physics of the nucleus: how deeply do cells 'feel' outside and in? *Journal of cell science*, 123:297–308, 2010.

[9] D.R. Carter, P.R. Blenman, and G.S. Beaupré. Correlations between mechanical stress history and tissue differentiation in initial fracture healing. *Journal of Orthopaedic Research*, 7:398–407, 1988.

[10] L.E. Claes and C.A. Heigele. Magnitudes of local stress and strain along bony surfaces predict the coarse and type of fracture healing. *Journal of Biomechanics*, 32:255–66, 1999.

[11] D.M. Cullinane, K.T. Salisbury, Y. Alkhiary, and S. Eisenberg. Effects of the local mechanical environment on vertebrate tissue differentiation during repair: does repair recapitulate development. *J. Exp. Biol.*, 206:2459–71, 2003.

[12] R.M. Delaine-Smith and C.R. Gwendolen. Mesenchymal stem cell responses to mechanical stimuli. *Muscles Ligaments Tendons J.*, 2(3):169–80, 2012.

[13] A.J. Engler, S. Sen, H.L. Sweeney, and D.E. Discher. Matrix elasticity directs stem cell lineage specification. *Cell*, 126:677–89, 2006.

[14] B. Trappmann et al. Extracellular-matrix tethering regulates stem-cell fate. *Nature Materials*, 11:642–9, 2012.

[15] L. Trichet et al. Evidence of a large-scale mechanosensing mechanism for cellular adaptation to substrate stiffness. *Proc Natl Acad Sci*, 109(18):6933–38, 2012.

[16] N.D. Evans, C. Minelli, E. Gentleman, V. LaPointe, S.N. Patankar, M. Kallivretaki, X. Chen, C.J. Roberts, and M.M. Stevens. Substrate stiffness affects early differentiation events in embryonic stem cells. *Eur. Cell Mater*, 18:1–14, 2009.

[17] S. Faghihi, A. Karimi, M. Jamadi, R. Imani, and R. Salarian. Graphene oxide/poly(acrylic acid)/gelatin nanocomposite hydrogel: experimental and numerical validation of hyperelastic model. *Mater Sci Eng C Mater Biol Appl*, 38:299–305, 2014.

[18] S. Fouliarda, S. Benhamidaa, N. Lenuzzab, and F. Xaviera. Modeling and simulation of cell populations interaction. *Mathematical and Computer Modelling*, 49(11):2104–8, 2009.

[19] J.C. Friedland, M.H. Lee, and D. Boettiger. Mechanically activated integrin switch controls $\alpha 5\beta 1$ function. *Science*, 323:642–44, 2009.

[20] J. Fu, Y.K. Wang, M.T. Yang, R.A. Desai, X. Yu, Z. Liu, and C.S. Chen. Mechanical regulation of cell function with geometrically modulated elastomeric substrates. *Nature Methods*, 7:733–736, 2010.

[21] L. GERIS, H. VAN OOSTERWYCK, J. VANDER SLOTEN, J. DUYCK, and I. NAERT. Assessment of mechanobiological models for the numerical simulation of tissue differentiation around immediately loaded implants. *Comput Methods Biomech Biomed Engin.*, 6:277–88, 2003.

[22] S.J. Gladman, R.E. Ward, A.T. Michael-Titus, M.M. Knight, and J.V. Priestley. The effect of mechanical strain or hypoxia on cell death in subpopulations of rat dorsal root ganglion neurons in vitro. *Neuroscience*, 171(2):577–87, 2010.

[23] N.C. Harrison, R.D. del Corral, and B. Vasiev. Coordination of cell differentiation and migration in mathematical models of caudal embryonic axis extension. *PLoS ONE*, 6:e22700, 2011.

[24] G.J. Hera, H.Ch. Wub, M.H. Chenc, M.Y. Chene, Sh.Ch. Change, and T.W. Wanga. Control of three-dimensional substrate stiffness to manipulate mesenchymal stem cell fate toward neuronal or glial lineages. *Acta Biomaterialia*, 9(2):5170–80, 2013.

[25] Hibbit, Karlson, and Sorensen. *Abaqus-Theory manual*, 6.11-3 edition edition, 2011.

[26] N. Huebsch, P.R. Arany, A.S. Mao, D. Shvartsman, O.A. Ali, S.A. Bencherif, J. Rivera-Feliciano, and D.J. Mooney. Harnessing traction-mediated manipulation of the cell/matrix interface to control stem-cell fate. *Nat. Mater.*, 9:518–26, 2010.

[27] H. Isaksson, W. Wilson, C.C. van Donkelaar, R. Huiskes, and K. Ito. Comparison of biophysical stimuli for mechano-regulation of tissue differentiation during fracture healing. *J Biomech.*, 39(8):1507–16, 2006.

[28] D.W. James and J.F. Taylor. The stress developed by sheets of chick fibroblasts in vitro. *Experimental Cell Research*, 54:107–110, 1969.

[29] A.K. Jha, W.M. Jackson, and K.E. Healy. Controlling osteogenic stem cell differentiation via soft bioinspired hydrogels. *PLoS ONE*, 9(6):e98640, 2014.

[30] K.T. Kang, J.H. Park, H.J. Kim, H.M. Lee, K.-I. Lee, H.H. Jung, H.Y. Lee, Y.B. Shim, and J.W. Jang. Study on differentiation of mesenchymal stem cells by mechanical stimuli and an algorithm for bone fracture healing. *Tissue Engineering and Regenerative Medicine*, 8(4):359–70, 2011.

[31] E.M. Kearney, P.J. Prendergast, and V.A. Campbell. Mechanisms of strain-mediated mesenchymal stem cell apoptosis. *J Biomech Eng*, 130(6):061004, 2008.

[32] D.J. Kelly and P.J. Prendergast. Mechano-regulation of stem cell differentiation and tissue regeneration in osteochondral defects. *Journal of Biomechanics*, 38(7):1413–22, 2005.

[33] A. Kunze, P. Tseng, C. Murray, A. Caputo, F.E. Schweizer, and D. Di Carlo. Micro magnet chips to study nanoparticle force-induced neural cell migration. *17th International Conference on Miniaturized Systems for Chemistry and Life Sciences 27-31 October*, pages 431–3, 2013.

[34] K. Kurpinski, J. Chu, C. Hashi, and S. Li. Anisotropic mechanosensing by mesenchymal stem cells. *Proc Natl Acad Sci USA*, 103(44):16095–100, 2006.

[35] K. Kurpinski, J. Chu, D. Wang, and S. Li. Proteomic profiling of mesenchymal stem cell responses to mechanical strain and TGF-$\beta 1$. *Cell Mol Bioeng.*, 2(4):606–14, 2009.

[36] D. Lacroix and P.J. Prendergast. A mechano-regulation model for tissue differentiation during fracture healing: analysis of gap size and loading. *Journal of Biomechanics*, 35:1163–71, 2002.

[37] D. Lacroix, P.J. Prendergast, G. Li, and D. Marsh. Biomechanical model of simulate tissue differentiation and bone regeneration: application to fracture healing. *Medical and Biological Engineering and Computing*,

40:14–21, 2002.

[38] D.A. Lee, M.M. Knight, J.J. Campbell, and D.L. Bader. Stem cell mechanobiology. *J Cell Biochem.*, 112(1):1–9, 2011.

[39] Y. Lee, J. Huang, Y. Wangc, and K. Lin. Three-dimensional fibroblast morphology on compliant substrates of controlled negative curvature. *Integr. Biol.*, page 10.1039/C3IB40161H, 2013.

[40] D. Li, J. Zhou, F. Chowdhury, J. Cheng, N. Wang, and F. Wang. Role of mechanical factors in fate decisions of stem cells. *Regen Med.*, 6(2):229–40, 2011.

[41] C.M. Lo, H.B. Wang, M. Dembo, and Y.L. Wang. Cell movement is guided by the rigidity of the substrate. *Biophysical Journal*, 79:144–152, 2000.

[42] R.A. Marklein and J.A. Burdick. Spatially controlled hydrogel mechanics to modulate stem cell interactions. *Soft Matter*, 6:136–143, 2010.

[43] T.M. Maul, D.W. Chew, A. Nieponice, and D.A. Vorp. Mechanical stimuli differentially control stem cell behavior: morphology, proliferation, and differentiation. *Biomech Model Mechanobiol.*, pages 939–53, 2011.

[44] P. Moreo, J.M. Garcia-Aznar, and M. Doblaré. Modeling mechanosensing and its effect on the migration and proliferation of adherent cells. *Acta Biomaterialia*, 4:613–621, 2008.

[45] S.J. Mousavi, M. Doblaré, and M.H. Doweidar. Computational modelling of multi-cell migration in a multi-signalling substrate. *Physical Biology*, 11(2):026002 (17pp), 2014.

[46] S.J. Mousavi and M.H. Doweidar. A novel mechanotactic 3D modeling of cell morphology. *J Phys Biol*, 11(4):046005, 2014.

[47] S.J. Mousavi and M.H. Doweidar. Role of mechanical cues in cell differentiation and proliferation: A 3d numerical model. *PLoS One*, 10(5):e0124529, 2015.

[48] S.J. Mousavi, M.H. Doweidar, and M. Doblaré. Computational modelling and analysis of mechanical conditions on cell locomotion and cell-cell interaction. *Comput Methods Biomech Biomed Engin.*, page DOI: 10.1080/10255842.2012.710841, 2012.

[49] S.J. Mousavi, M.H. Doweidar, and M. Doblaré. 3D computational modelling of cell migration: A mechano-chemo-thermo-electrotaxis approach. *J. Theor. Biol*, 329:64–73, 2013.

[50] S.J. Mousavi, M.H. Doweidar, and M. Doblaré. Cell migration and cell-cell interaction in the presence of mechano-chemo-thermotaxis. *Mol Cell Biomech.*, 10(1):1–25, 2013.

[51] S..J Mousavi and Doweidar M.H. Three-dimensional numerical model of cell morphology during migration in multi-signaling substrates. *Plos One*, 10(3):e0122094, 2015.

[52] S. Nagaoka, H. Tanzawa, and J. Suzuki. Cell proliferation on hydrogels. *In Vitro Cell Dev Biol*, 26(1):51–6, 1990.

[53] R. W. Ogden. *Nonlinear Elastic Deformations*. Dover, 1998.

[54] G.F. Oster, J.D. Murray, and A.K. Harris. Mechanical aspects of mesenchymal morphogenesis. *J Embryol Exp Morphol.*, 78:83–125, 1983.

[55] K.T. Palomares, R.E. Gleason, Z.D. Mason, D.M. Cullinane, T.A. Einhorn, L.C. Gerstenfeld, and E.F. Morgan. Mechanical stimulation alters tissue differentiation and molecular expression during bone healing. *J Orthop Res.*, 27(9):1123–32, 2009.

[56] E. Palsson. A three-dimensional model of cell movement in multicellular systems. *Future Generation Computer System*, 17:835–852, 2001.

[57] C.G. Penelope and P.A. Janmey. Cell type-specific response to growth on soft materials. *Journal Applied Physiology*, 98:1547–1553, 2005.

[58] J.H. Pierce, E. Di Marco, G.W. Cox, D. Lombardi, M. Ruggiero, L. Varesio, L.M. Wang, G.G. Choudhury, A.Y. Sakaguchi, P.P. Di Fiore, and S.A. Aaronson. Macrophage-colony-stimulating factor (CSF-1) induces proliferation, chemotaxis, and reversible monocytic differentiation in myeloid progenitor cells transfected with the human c-fms/CSF-1 receptor cDNA. *Proc Natl Acad Sci*, 87(15):5613–7, 1990.

[59] M.F. Pittenger, A.M. Mackay, S.C. Beck, R.K. Jaiswal, R. Douglas, J.D. Mosca, M.A. Moorman, D.W. Simonetti, S. Craig, and D.R. Marshak. Multilineage potential of adult human mesenchymal stem cells. *Science*, 284(5411):143–7, 1999.

[60] P.A. Prokharaua, F.J. Vermolena, and J.M. Garcia-Aznar. A mathematical model for cell differentiation, as an evolutionary and regulated process. *Comput Methods Biomech Biomed Engin.*, 17(10):1051–70, 2014.

[61] S. Ramtani. Mechanical modelling of cell/ECM and cell/cell interactions during the contraction of a fibroblast-populated collagen microsphere:theory and model simulation. *Journal of Biomechanics*, 37:1709–1718, 2004.

[62] A. Schäfer and M. Radmacher. Influence of myosin ii activity on stiffness of fibroblast cells. *Acta Biomaterialia*, 1:273–280, 2005.

[63] H. Shen, S. Tong, G. Bao, and B. Wang. Structural responses of cells to intracellular magnetic force induced by superparamagnetic iron oxide nanoparticles. *Phys Chem Chem Phys*, 16(5):1914–20, 2014.

[64] A.J. Stops, K.B. Heraty, M. Browne, F.J. O'Brien, and P.E. McHugh. A prediction of cell differentiation and proliferation within a collagen-glycosaminoglycan scaffold subjected to mechanical strain and perfusive fluid flow. *J Biomech.*, 43(4):618–26, 2010.

[65] D.L. Taylor, J. Heiple, Y.L. Wang, E.J. Luna, L. Tanasugarn, J. Brier, J. Swanson, M. Fechheimer, P. Amato, M. Rockwel, and G. Daley. Cellular and molecular aspects of amoeboid movement. *CSH Symp. Quant. Biol.*, 46:101–111, 1982.

[66] M. Théry and M. Bornens. Cell shape and cell division. *Current Opinion in Cell Biology*, 18(6):648–57, 2006.

[67] T.A. Ulrich, E.M. De Juan Pardo, and S. Kumar. The mechanical rigidity of the extracellular matrix regulates the structure, motility, and proliferation of glioma cells. *Cancer Research*, 69:4167–4174, 2009.

[68] T. Wang, W. Sun, X. Liu, C. Wang, S. Fu, and Tong Z. Promoted cell proliferation and mechanical relaxation of nanocomposite hydrogels prepared in cell culture medium. *Reactive and Functional Polymers*, 73(5):683–9, 2013.

[69] M.A. Wozniak and C.S. Chen. Mechanotransduction in development: a growing role for contractility. *Nat. Rev. Mol. Cell. Biol.*, 10:34–43, 2009.

[70] Q.Q. Wu and Q. Chen. Mechanoregulation of chondrocyte proliferation, maturation, and hypertrophy: Ion-channel dependent transduction of matrix deformation signals. *Exp Cell Res.*, 256(2):383–91, 2000.

[71] M.H. Zaman, R.D. Kamm, P. Matsudaira, and D.A. Lauffenburgery. Computational model for cell migration in three-dimensional matrices. *Biophysical Journal*, 89:1389–1397, 2005.

[72] A. Zemel, F. Rehfeldt, A.E. Brown, D.E. Discher, and S.A. Safran. Optimal matrix rigidity for stress fiber polarization in stem cells. *Nat. Phys.*, 6:468–473, 2010.